

Indirect Determination of Material Properties of Closed-Cell Metal Foam: Comparison of Voxel and Tetrahedral Finite Element Models

O. Jiroušek, P. Koudelka and P. Zlámal
Department of Biomechanics
Institute of Theoretical and Applied Mechanics, v.v.i.
Academy of Sciences of the Czech Republic, Prague, Czech Republic

Abstract

In this paper a comprehensive evaluation of the microstructural finite element (micro-FE) models of closed-cell aluminum metal foam is given. Comparison of models developed using high resolution three-dimensional image data obtained using microtomographic scanning of a sample with different resolutions is presented. Two sets of micro-finite element models are prepared using the same image data: i) voxel finite element models in which every 3-D pixel (voxel) is directly converted to one hexahedral element and ii) tetrahedral finite element models which are prepared by filling a triangular surface mesh of the foam's microstructure.

A virtual uni-axial compression test is simulated in three mutually perpendicular directions to obtain the elastic moduli and the maximum values of the principal stresses as well as to quantify the anisotropy of the back-calculated material characteristics. The material model used in the finite element simulations is based on previously published results obtained from an experimental-numerical study of the base material used for production of the reference foam.

The elastic constants acquired from the finite element simulations of the most detailed models are in good agreement with the experimental results provided that the overall porosity of the material is well represented by the finite element models. The requirements in terms of the minimal spatial resolution of the microtomographic images needed for proper estimation of elastic properties of a closed-cell metal foams are given. The superiority of the voxel finite element models over the tetrahedral models is clearly demonstrated in the paper. The results obtained using tetrahedral finite element models at the lower resolution are poor compared with results obtained from the voxel models with the same resolution.

Keywords: metal foam, closed-cell material, orthotropic material properties, indirect methods, micro-CT, voxel models, tetrahedral models.

1 Introduction

Mechanical properties of geometrically complex materials can be investigated non-destructively using microfocus Computed Tomography (micro-CT) using inverse modeling. This involves development of FE model of the sample and performing a “virtual experiment“, i.e. computer simulation of the mechanical test. From the response of the finite element (FE) model to (usually unit) load, mechanical properties of the whole sample can be determined provided the material properties at the level of the microstructure are known. Results of such a simulation (and the calculated material properties) are dominantly influenced by the quality of the FE model. Basically, the microstructure of the material must be well represented by the FE model.

Generally there are three possibilities to generate FE models of a microstructure from 3D image data:

1. Convert each image voxel (3D pixel) directly to one hexahedral element. [1]
2. Find a smooth surface of the structure and fill the enclosed volume with tetrahedral elements [2]
3. Use a smoothed hexahedral mesh with mixed element types reflecting the smooth boundaries (pyramids, wedges and tetrahedras are present on the boundary of the enclosed volume) [3] [4]

For a material with very high porosity, such as the closed-cell metal foam, it is not an easy task to generate tetrahedral mesh of its microstructure. To find the smooth boundary of such a geometrically complex material a marching cubes algorithm is used [5] to find a set of connected triangles describing the surface. The surface is filled with tetrahedral elements using a Delaunay triangulation [6] extended to 3-D [7], [8]. Moreover, resulting microstructural FE models have very large number of degrees of freedom (DOFs) and the simulation of their deformation behavior can take days even on a modern computer.

It is therefore appropriate to use directly generated voxel models. The main advantage of the voxel FE models is that these models can be prepared automatically without any user intervention. The only assumption is that the quality of the 3-D images must be sufficient enough to enable automatic thresholding. Nevertheless, for a microstructure with such thin walls it is not obvious whether the voxel models can realistically describe the deformation behavior of the structure, neither is known at what resolution should the micro-CT images be taken to capture all the microstructural details.

Therefore, complex validation study of the modeling issues that might effect the results is necessary. In this work, large-scale tetrahedral FE models of the microstructure of a metal foam sample are compared with voxel models. These FE models are developed such as to reflect all possible effects which might influence the reliability and accuracy of results.

2 Materials and methods

2.1 Micro-CT scanning

A block sample of aluminum metal foam Alporas[®] with $25 \times 25 \times 25$ mm dimensions was scanned in a custom micro-CT device. Due to the very small thickness of the metal foam's walls, high-resolution scanning was necessary to capture the individual cell walls with possible defects. The sample was scanned in 0.5° increments using Hamamatsu L8601-01 microfocus X-ray tube (Hamamatsu Photonics K.K.) with $5 \mu\text{m}$ emission spot and a large-area flat panel X-ray detector Hamamatsu C7942CA-22 (Hamamatsu Photonics K.K.) with dimensions $120 \text{ mm} \times 120 \text{ mm}$ and resolution 2368×2240 pixels. Resolution of the reconstructed images was approximately $30 \mu\text{m}^3$ which is sufficient for capturing the geometrical details of such cellular material (typical wall thickness of the sample was $100 - 300 \mu\text{m}$).

Cross-sectional images were obtained using a cone-beam filtered backprojection reconstruction algorithm developed in Matlab environment [9] with the computational core (backprojector) written in C++ code to enable parallel processing on multiprocessor architectures.

2.2 Development of the micro-FE models

The images were converted to binary ones using adaptive threshold with global threshold value based on Otsu's algorithm [10] which chooses the threshold to minimize the intraclass variance of the black and white pixels. These binary images contained only the thin walls and were used for development both the tetrahedral and voxel FE models. For the voxel models, direct conversion of graphic voxels to FE elements was used. Effect of resolution of the input images was studied using set of images reconstructed from the acquired projections with six different levels of spatial resolutions. The full resolution of the base image data was $800 \times 800 \times 800$ pixels, remaining 3-D images were reconstructed in resolutions $400 \times 400 \times 400$, $320 \times 320 \times 320$, $240 \times 240 \times 240$, $160 \times 160 \times 160$ and $80 \times 80 \times 80$ pixels. Effects of the image resolution on segmented images is depicted in Fig. 1.

To enable comparison of models generated using the images with such a different resolution ($10 \times$ difference) the segmented thin walls of the foam had to be artificially grown thicker. If this artificial growing was not performed, it would not be possible to generate continuous FE models for the lower resolutions. This artificial growing has a consequence in lower porosity of the FE model compared to reality. This is later compensated by multiplying the resulting elastic constants by the ratio of real density to the density of the FE model. The authors are aware of the fact, that a change in porosity influences other results (e.g. stress distribution) significantly, but without the artificial growing the comparison would not be possible because of the discontinuity of both the voxel and tetrahedral FE models.

From the thresholded images six voxel FE models were generated simply by con-

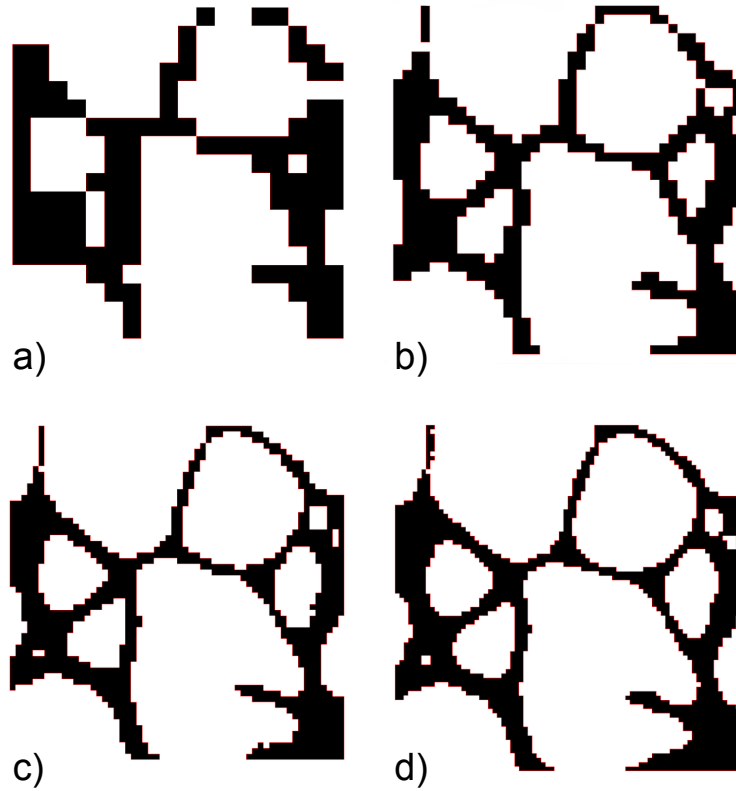


Figure 1: Effects of segmentation of the foam's microstructure using images with different resolution: a) $80 \times 80 \times 80$, b) $160 \times 160 \times 160$, c) $240 \times 240 \times 240$, d) $400 \times 400 \times 400$. Only small part of the microstructure is shown.

verting each voxel to 8-node hexahedral element. Porosity of these FE models together with number of nodes and elements is summarized in Tab. 1.

Model resolution	No. of elements	No. of nodes	Porosity
$80 \times 80 \times 80$	123,904	262,181	0.7580
$160 \times 160 \times 160$	761,040	1,372,756	0.8142
$240 \times 240 \times 240$	2,362,500	3,785,175	0.8291
$320 \times 320 \times 320$	5,423,104	7,994,418	0.8345
$400 \times 400 \times 400$	10,547,200	14,594,868	0.8352
$800 \times 800 \times 800$	84,019,200	100,539,069	0.8359

Table 1: Total number of elements, nodes and resulting porosity for generated voxel FE models

The most profound disadvantage of the hexahedral models is the coarse representation of their in reality smooth boundary. This disadvantage can be overcome by using hexahedral meshes with smoothed boundaries or using completely tetrahedral meshes.

In this work, only tetrahedral models were used. To develop these models the same binary image data were used to find the triangular surface which was in the second step filled with tetrahedral elements. A great care was taken to generate these models with total volume (and porosity) similar to their voxel counterparts. The details of the tetrahedral models are summarized in Tab. 2.

Model resolution	No. of elements	No. of nodes	Porosity
80×80×80	1,102,341	236,403	0.7087
160×160×160	5,813,196	1,261,436	0.8010
240×240×240	17,970,090	3,785,175	–
320×320×320 ^{*)}	35,191,552	7,380,954	–
400×400×400 ^{*)}	65,055,296	13,271,328	–
800×800×800 ^{*)}	119,634,762	24,892,161	–

Table 2: Total number of elements, nodes and resulting porosity for generated tetrahedral FE models. ^{*)} The number of elements and nodes were estimated based on smaller-size models ($\frac{1}{4}$ of the dimensions of the cube, i.e. using only $6 \times 6 \times 6 \text{ mm}^3$). It was not possible to build these models using the whole image data due to the extreme memory requirements ($>70 \text{ GB RAM}$).

2.3 Material properties at the cell–wall level

Alporas[®] is a closed-cell aluminium foam developed in late 80’s manufactured using batch casting process and produced by Japan manufacturer Shinko Wire Co., Ltd. Structure of this material is typically constituted by large inner pores of polyhedral shape with mean size $\sim 4.5 \text{ mm}$. Cell walls that create complex random inner structure are typically $100 \mu\text{m}$ thick with overall porosity approximately 90% [12], although it can be produced at different levels of porosity saying that polyhedron cells become spherical at porosities under 70%. Foam is manufactured using special unnormalized alloy containing 97% of aluminium, 1.5% of calcium and 1.5% of titanium [12].

Although material properties of this alloy are not provided by the manufacturer, its characteristics have been assessed in experimental-numerical study [13] resulting in $E = 68 \text{ GPa}$. Elastic modulus of the cell wall was measured in the range of a general alumina alloys ($E = 61.7\text{--}73.1 \text{ GPa}$) which was further verified by nanoindentation tests evaluated using Oliver and Pharr methodology together with deconvolution technique [11].

2.4 FE analysis

To compare ability of the FE models to predict overall material characteristics of Alporas a uni-axial unit compression tests in all three mutually perpendicular directions were simulated in ANSYS software. Young’s modulus of the foam’s material (68 GPa)

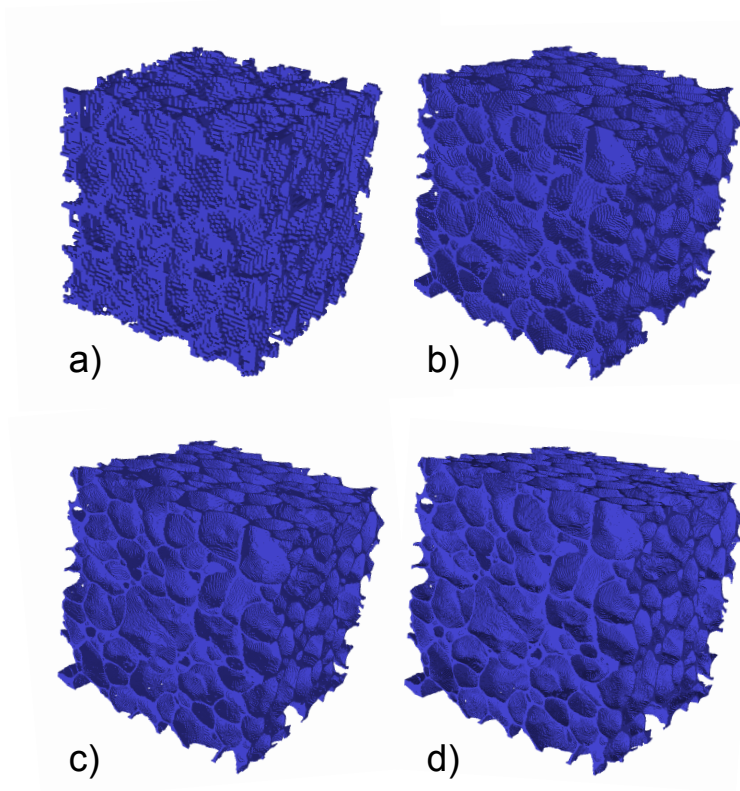


Figure 2: Generated voxel FE models with different levels of spatial resolution: a) $80 \times 80 \times 80$, b) $160 \times 160 \times 160$, c) $240 \times 240 \times 240$, d) $400 \times 400 \times 400$.

was taken from literature [13] as well as the Poisson's ratio $\nu = 0.33$ [12]. The unit loading was prescribed as a given displacement of the top (side) area of the cube as to invoke unit strain in the sample. The opposite surface of the sample was prescribed rigid boundary conditions.

Overall mechanical properties were calculated as the applied force (calculated as the sum of reactions at the fixed end) divided by the cross-sectional area of the sample. Comparison of orthotropic elastic properties (E_x, E_y, E_z), maximal values of principal stresses ($\sigma_1, \sigma_2, \sigma_3$) as well as magnitudes and locations of localized deformations were performed for all the studied FE models.

3 Results

For all the studied FE models of the Alporas foam reaction forces in the fixed end as well as maximal values of principal stresses and strains were written in text files. The principal stresses were determined in the middle part of the sample only (1/3 of the dimension of the sample in the direction of loading) to avoid the effect of boundary conditions. Selected results obtained from these simulations are summarized in Tab. 3.

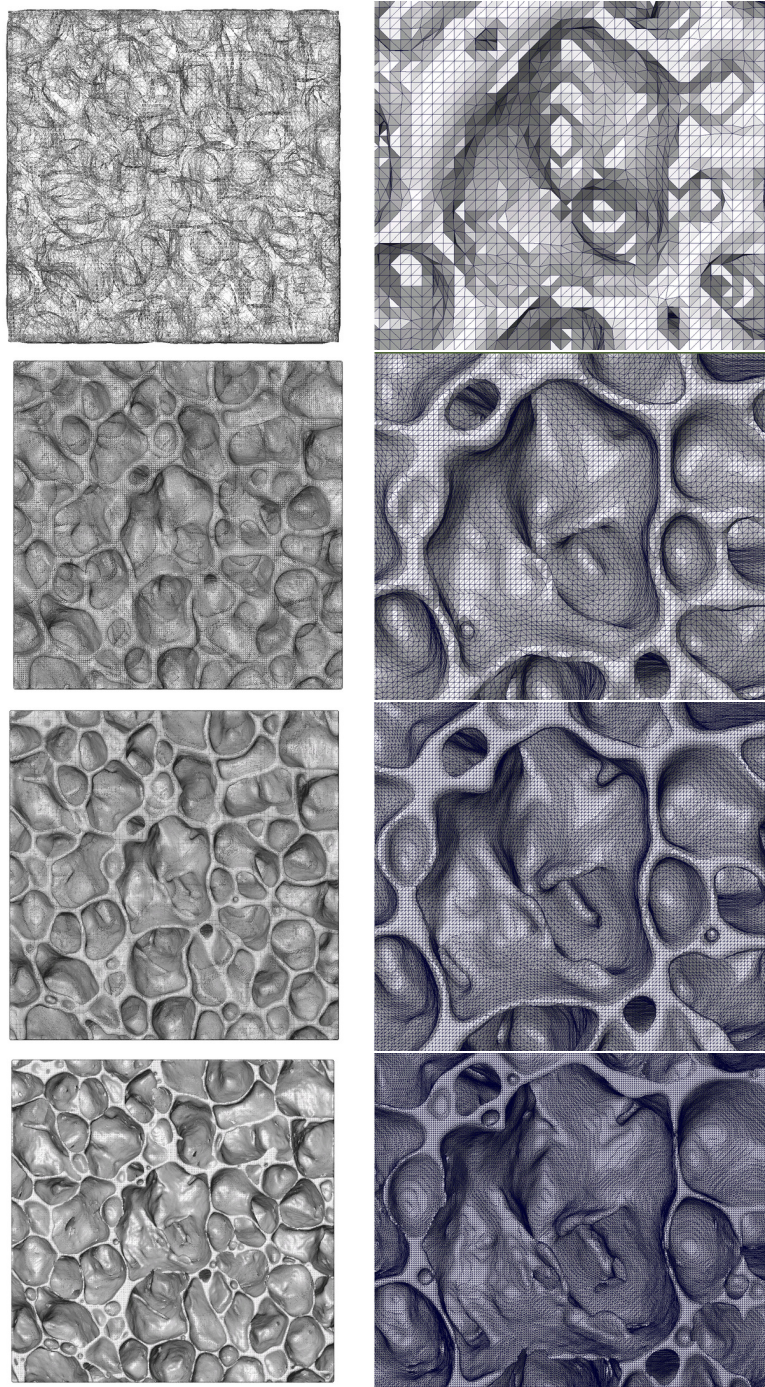


Figure 3: Tetrahedral FE models of the foam generated from the binary images with the same spatial resolution as in case of the voxel models. Front side of the 25 mm^3 cube (left) and a zoomed central part, corresponding to approximately $\frac{1}{9}$ of the area (right). Due to their complexity, only models developed from $80 \times 80 \times 80$, $160 \times 160 \times 160$, $240 \times 240 \times 240$ and $400 \times 400 \times 400$ image data are shown.

Size [px]	E [GPa]			Principal stresses [MPa]					
	E_x	E_y	E_z	σ_{1x}^{max}	σ_{3x}^{min}	σ_{1y}^{max}	σ_{3y}^{min}	σ_{1z}^{max}	σ_{3z}^{min}
80 ³	5.40	4.30	5.82	933.0	-1,610.0	1,038.2	-1,457.2	1,315.5	-2129.9
160 ³	4.20	4.39	4.57	1,276.5	-2,014.1	815.9	-1,635.8	879.2	-1823.5
240 ³	3.84	3.23	4.19	981.8	-1,908.5	869.6	-2,110.8	990.8	-2377.6
320 ³	3.70	2.78	4.05	972.5	-2,458.5	1,145.4	-1,845.9	972.5	-2458.4
400 ³	3.61	2.78	4.07	983.7	-2,509.3	953.5	-2,006.8	990.9	-2683.4
800 ³	–	–	–	–	–	–	–	–	– ^{**)}

Table 3: Overall material properties for voxel FE models together with maximal values of principal stresses. ^{**)} These values were not computed because of the model size ($\sim 3.10^9$ unknowns).

Calculated values of elastic moduli are much higher than experimentally obtained ones. This is caused by the over-segmentation of the images that was necessary to build the FE models with lower resolutions as discussed in section 2.1. However, the over-segmentation is not necessary and was used here only to enable the direct comparison of the models. To get closer to the experimentally obtained values of material properties one can multiply the results by the proportion between the real porosity and porosity of the FE model. This multiplication leads to much realistic material properties of the aluminum foam as given in Tab. 4.

Size	Porosity	Real porosity	Ratio	E_x [GPa]	E_y [GPa]	E_z [GPa]
80 ³	0.7580	0.91	2.69	2.01	1.63	2.16
160 ³	0.8142	0.91	2.06	2.04	1.57	2.21
240 ³	0.8291	0.91	1.90	2.02	1.53	2.21
320 ³	0.8345	0.91	1.84	2.01	1.51	2.20
400 ³	0.8352	0.91	1.83	2.00	1.52	2.22
800 ³	0.8359	0.91	1.82	–	–	–

Table 4: Overall orthotropic material properties adapted according to real porosity (voxel models)

The same approach was used for the tetrahedral models. The models describe the complex microstructure with a greater detail, especially for the higher resolution of the input image data. The complexity is clearly demonstrated in Fig. 3. Regardless to the higher detail of the tetrahedral models and larger number of unknowns, it is clear from Tab. 5 that prediction of elastic properties with tetrahedral models is much poorer. This is mainly caused by the well known fact, that linear tetrahedral elements often yield an inaccurate solution in critical regions due to their high distortion. For the tetrahedral FE models built over the images with lowest resolution it was not possible to guarantee good quality of the tetrahedrons.

To reflect the problem with over-segmentation, similar approach was used as in

Size [px]	E [GPa]			Principal stresses [MPa]					
	E_x	E_y	E_z	σ_{1x}^{max}	σ_{3x}^{min}	σ_{1y}^{max}	σ_{3y}^{min}	σ_{1z}^{max}	σ_{3z}^{min}
80 ³	19.56	18.25	17.04	419.5	-1,273.2	358.9	-1,110.1	265.1	-1,188.3
160 ³	10.54	12.55	13.43	595.6	-1,700.4	575.2	-1,719.2	425.8	-1,841.1
240 ³	8.96	10.97	11.89	471.7	-1,572.0	511.8	-1,410.3	398.1	-1,423.7
320 ³ *)	–	–	–	–	–	–	–	–	–
400 ³ *)	–	–	–	–	–	–	–	–	–
800 ³ *)	–	–	–	–	–	–	–	–	–

Table 5: Overall material properties for tetrahedral FE models together with maximal values of principal stresses. *) These values were not computed because of the memory required to build these models (>70 GB RAM).

voxel models. The total volume of the model was computed as the sum of volumes of individual tetrahedras. Porosity was computed as the total volume of all tetrahedras divided by volume of the enclosing cube. However, results shown in Tab. 6 indicate that tetrahedral models have poor prediction of elastic properties compared to voxel models of comparable number of elements/nodes.

Size	Porosity	Real porosity	Ratio	E_x [GPa]	E_y [GPa]	E_z [GPa]
80 ³	0.7087	0.91	3.24	6.04	5.64	5.27
160 ³	0.8010	0.91	2.21	3.26	3.88	4.15
240 ³	0.1902	0.09	2.11	2.77	3.39	3.67
320 ³ *)	–	–	–	–	–	–
400 ³ *)	–	–	–	–	–	–
800 ³ *)	–	–	–	–	–	–

Table 6: Overall orthotropic material properties adapted according to real porosity (tetrahedral models). *) These values were not computed because of the memory requirements.

It is obvious that coarse tetrahedral models are not suitable for indirect determination of material properties of the studied material. Multiplication of the results by the proportion between the real porosity and porosity of the FE model leads to elastic moduli significantly higher than actual values of the reference material. Furthermore, results exhibit apparent stochastic scatter in individual spatial directions. Although tetrahedral models with the spatial resolution of $320 \times 320 \times 320$ and greater have very good ability to predict the elastic material properties, it is impractical to use these meshes due to computational time and related hardware requirements (only generation of the model required more than 70 GB RAM).

4 Conclusion

In this paper a comprehensive comparison of FE models of the microstructure of metal foam was presented. The models were developed using high-resolution micro-CT image data of a cubic sample of the foam with dimensions of representative volume element. Calculation of overall material properties of the foam was performed using inverse FE simulation of compressive test performed in three mutually orthogonal directions. Orthotropic elastic properties as well as values of the principal stresses were compared for all the considered models. There are several conclusions which can be drawn from these FE simulations:

When one needs to estimate the *elastic* orthotropic properties voxel FE models can be successfully used, provided that the resolution of the image data is at least equal to the minimal wall thickness. In our computations, the model with $160 \times 160 \times 160$ pixel resolution corresponds to $100 \mu\text{m}^3$ resolution, which is in agreement with our findings (typical wall thickness for the scanned sample of Alporas foam was $100 - 300 \mu\text{m}$). For the voxel FE models, further improvement of the image data and thus better segmentation had almost no effect on the resulting elastic properties provided that the real porosity of the sample is well captured by the FE model.

The importance of proper image segmentation and minimal requirements for the resolution of the input images is clearly demonstrated by the results obtained. Elastic properties indirectly calculated by the FE simulations of the most detailed models show good correspondence with experiments (performed only in one direction) and are also in good correspondence with both experimental results and production characteristics of Alporas.

Acknowledgment

The research has been supported by RVO: 68378297 and by the Czech Science Foundation (grant No. P105/12/0824).

References

- [1] M. Lengsfeld, J. Schmitt, P. Alter, J. Kaminsky, R. Leppek, "Comparison of geometry-based and CT voxel-based finite element modelling and experimental validation", *Medical Engineering & Physics*, 20, 7, 515–522, 1998.
- [2] M. Viceconti, L. Bellingeri, L. Cristofolini, A. Toni, "A comparative study on different methods of automatic mesh generation of human femurs", *Medical Engineering & Physics*, 20, 1, 1–10, 1998.
- [3] W. Min, "Generating Hexahedron-Dominant Mesh Based on Shrinking-Mapping Method", *Proceedings of the 6th International Meshing Roundtable*, Park City, Utah, Sandia National Laboratories, 171–182, 1997.

- [4] S. K. Boyd, R. Muller, “Smooth surface meshing for automated finite element model generation from 3D image data“, *Journal of Biomechanics*, 39, 7, 1287–1295, 2006.
- [5] W. E. Lorensen, H. E. Cline, “Marching Cubes: A high resolution 3D surface construction algorithm“, *Computer Graphics*, 21, 4, pp. 163–169, 1987.
- [6] B. Delaunay, “Sur la sphre vide“, *Izvestia Akademii Nauk SSSR, Otdelenie Matematicheskikh i Estestvennykh Nauk*, 7, 793-800, 1934.
- [7] L. P. Chew, “Constrained Delaunay Triangulation“, *Algorithmica*, 4, 1, 97–108, 1989.
- [8] J. R. Shewchuk, “Tetrahedral Mesh Generation by Delaunay Refinement“, *Proceedings of the Fourteenth Annual Symposium on Computational Geometry (Minneapolis, Minnesota)*, 86–95, 1998.
- [9] D. Vavřík, P. Soukup, “Metal grain structure resolved with table-top microtomographic system“, *Journal of Instrumentation*, 6, 11, 1–7, 2011.
- [10] N. Otsu, “A Threshold Selection Method from Gray-Level Histograms“, *IEEE Transactions on Systems, Man, and Cybernetics*, 9, 1, 62–66, 1979.
- [11] V. Králík, J. Němeček, “Two-scale model for prediction of macroscopic elastic properties of aluminium foam“, *Chemické Listy*, 105, 17, 672–675, 2011.
- [12] T. Miyoshi, M. Itoh, S. Akiyama, A. Kitahara, “Aluminium foam, ‘ALPORAS’: The Production Process, Properties and Applications“, *Materials Research Society Symposium Proc.*, 521, 1998.
- [13] I. Jeon, K. Katou, T. Sonoda, T. Asashina, K-J. Kang, “Cell wall mechanical properties of closed-cell Al foam“, *Mechanics of Materials*, 41, 1, 60–73, 2009.